crystals

MDPI

Article

Optimizing the Rolling Process of Lightweight Materials

Jessica Rawles *, Svitlana Fialkova, Kai Hubbard, Zhigang Xu, Christopher Hale and Jagannathan Sankar

check for updates

Citation: Rawles, J.; Fialkova, S.; Hubbard, K.; Xu, Z.; Hale, C.; Sankar, J. Optimizing the Rolling Process of Lightweight Materials. *Crystals* **2024**, *14*, 582. https://doi.org/10.3390/cryst14070582

Academic Editor: Mingyi Zheng

Received: 28 May 2024
Revised: 20 June 2024
Accepted: 23 June 2024
Published: 25 June 2024

Mechanical Engineering, North Carolina Agricultural and Technical State University, Greensboro, NC 27411, USA; sfialkov@ncat.edu (S.F.); kmhubbard@aggies.ncat.edu (K.H.); zhigang@ncat.edu (Z.X.); clhale@ncat.edu (C.H.); sankar@ncat.edu (J.S.)
* Correspondence: jlrawles@aggies.ncat.edu

Abstract: Conventional rolling is a plastic deformation process that uses compression between two rolls to reduce material thickness and produce sheet/plane geometries. This deformation process modifies the material structure by generating texture, reducing the grain size, and strengthening the material. The rolling process can enhance the strength and hardness of lightweight materials while still preserving their inherent lightness. Lightweight metals like magnesium alloys tend to lack mechanical strength and hardness in load-bearing applications. The general rolling process is controlled by the thickness reduction, velocity of the rolls, and temperature. When held at a constant thickness reduction, each pass through the rolls introduces an increase in strain hardening, which could ultimately result in cracking, spallation, and other defects. This study is designed to optimize the rolling process by evaluating the effects of the strain rate, rather than the thickness reduction, as a process control parameter.

Keywords: lightweight materials; conventional rolling; metal forming; warm working; manufacturing optimization

1. Introduction

Lightweight metals and alloys are highly valued in the automotive, aerospace, and medical industries for their excellent strength-to-weight ratios. These properties are ideal for applications that prioritize fuel efficiency and energy conservation. Titanium and magnesium alloys have been studied extensively for lightweight applications. Magnesium is the lightest of all structural metals, with a density that is one-quarter that of steel [1]. Although Mg-based alloys typically exhibit lower strength and ductility compared to other structural metals, the addition of alloying elements can yield materials with an excellent strength-to-weight ratio, good fatigue and impact strengths, and relatively high thermal and electrical conductivities [2]. Titanium (Ti) alloys also present favorable characteristics, including high strength, corrosion resistance, and reliable mechanical properties at elevated temperatures.

Aluminum is a common alloying element in both magnesium and titanium. Magnesium–aluminum alloys are valued for their low density, making them ideal for lightweight applications. Adding aluminum to magnesium increases hardness, strength, and formability while having a minimal impact on density [3]. When aluminum dissolves in α-Mg, it induces solid solution strengthening. However, a higher aluminum content leads to the formation of the hard and brittle intermetallic phase $Al_{12}Mg_{17}$, which is undesirable due to its hardness, brittleness, and low thermal stability [4,5]. The fragility at the Mg/$Al_{12}Mg_{17}$ interface stems from a mismatch in crystal structures: α-Mg has a hexagonal close-packed (HCP) arrangement, whereas γ-$Al_{12}Mg_{17}$ has a body-centered cubic (BCC) structure [6].

Ti-6Al-4V is a dual-phase (α + β) titanium alloy that incorporates aluminum and vanadium as substitutional elements. The α and β of this alloy have different crystal structures. The α phase Ti-6Al-4V is stable under 650 °C and has an HCP structure while the β phase occurs at temperatures above 900 °C and is of BCC structure [7]. Compared to pure titanium, Ti-6Al-4V exhibits greater hardness, yield strength, and tensile strength, with a tensile yield strength of 900 MPa [8]. This alloy has a superior strength-to-weight ratio, excellent corrosion resistance, and ease of machinability [8,9]. However, due to its high strength and limited formability, Ti-6Al-4V is typically processed at high temperatures, which can be costly.

Enhancing the strength and ductility of lightweight alloys through plastic deformation processes can improve material sustainability and durability while maintaining a low weight. Grain refinement, a common method to enhance material properties, can be achieved through severe plastic deformation techniques such as conventional rolling, cold rolling, hard-plate rolling, and ultrasonic surface rolling. Bulk forming processes like rolling produce deformation textures

influenced by the strain path during processing. Rolling processes typically result in a texture similar to plain strain tension, with compression being the primary stress state.

The cold rolling of magnesium alloys leads to a high density of dislocations and deformation twins, significantly contributing to strain hardening. This process can adversely affect the anisotropic behavior due to the development of a strong basal texture [10,11]. However, the strain hardening from cold rolling also increases the yield strength and tensile strength of the Mg alloys. Additionally, cold rolling increases the hardness of Mg alloys, making them more susceptible to brittle cracking. Ti alloys processed through cold rolling experience significant deformation as well as a high density of dislocations. The process of strain hardening the alpha phase in titanium alloys results in a more refined microstructure, which in turn leads to a rise in dislocation density. Similar to magnesium, titanium alloys sacrifice ductility through cold rolling in exchange for increased strength and hardness. Hard plate rolling, being a cold rolling process, exhibits similar effects on both magnesium and titanium alloys to those observed in traditional cold rolling techniques.

Ultrasonic surface rolling (USRP) is similar to conventional rolling but incorporates ultrasonic vibration. This technique aims to enhance the fatigue performance of metallic materials by improving their surface properties. The plastic deformation induced by USRP results in grain refinement and increased dislocation density. In magnesium alloys, USRP creates ultra-fine grain structures on the surface, leading to a more uniform microstructure. This process improves the surface hardness by up to 50% in some Mg alloys and by more than 50% in some Ti alloys [12]. The enhancements in fatigue performance are due to the compressive residual stress induced by USRP. In titanium alloys, USRP promotes the formation of a nanocrystalline surface layer, resulting in reduced surface roughness. The improvement in the surface hardness and fatigue life of titanium alloys after USRP can be attributed to the compressive residual stresses introduced by the process. These stresses make titanium alloys less susceptible to crack initiation and propagation under cyclic loading [13].

Conventional rolling is a plastic deformation process in which the dislocation of polycrystalline material structure is initiated through the stress applied by two compressive rolls [14,15]. In plastic deformation processes, continuous dislocation induces changes in the grain morphology, ultimately leading to an augmentation in the overall grain boundary area. The increase in dislocations can also be attributed to internal structures within the grains such as secondary phases [16]. These secondary phases deform less readily and sometimes not at all and tend to be more brittle in nature. The crystal orientation tends to correspond to the direction of the applied stress establishing the preferred orientation and generating texture. The energy stored from dislocation and increased grain boundary area is what causes the strengthening of material through plastic deformation [17]. For this study, conventional rolling was the preferred deformation process because it minimizes the critical shear stress and is less likely to initiate stress-induced phase transformation.

Deformation mechanisms in metallic structures are often linked to the strain rate sensitivity, defined as the variation of flow stress with increasing strain rate. Key parameters influencing the strain rate sensitivity include the deformation temperature, texture or grain size, and deformation velocity. As the deformation temperature rises, the strain rate sensitivity increases more rapidly compared to room temperature conditions. Dislocations, which cause the reorientation of crystals within a metallic structure, generate texture in plastically deformed alloys. The crystallographic orientation, deformation modes, and slip systems significantly influence the strain. Complex slip systems limit dislocations, and fewer dislocation sites increase the likelihood of concentrated strain in plastically deformed regions [18].

During severe plastic deformation, dislocations tend to move along the slip plane's direction, and this movement also relies on the direction in which the stress is applied. The direction of slip typically corresponds with the most densely packed plane. Typically, under ambient conditions, both magnesium and titanium alloys exhibit a hexagonal close-packed (HCP) crystal structure. HCP polycrystalline materials have limited deformation systems, which has a negative impact on material ductility. HCP structures are sensitive to the crystallographic texture because of their low symmetry and anisotropic behavior [19,20]. This results in a significant effect on texture evolution for HCP material during plastic deformation. Material texture generated for rolling HCP crystals is heavily dictated by the level of impurities, the effect of the c/a ratio of the crystal cell, and the initial texture.

The HCP crystal structure has a limited number of slip systems, which leads to reduced ductility when subjected to severe plastic deformation. For material like Ti that have a lower than ideal (1.6333) c/a ratio, the preferred slip system during deformation is along the prismatic plane. Whereas for Mg alloys, basal slip (0001) is the preferred direction of deformation because of its high c/a ratio [16,21,22]. During plastic deformation, mechanical twinning of Mg occurs on the $\{10\bar{1}2\}$ planes in the $\langle 10\bar{1}1\rangle$ direction, specifically observed under c-axis tension. The formability of Mg is limited by its insufficient slip systems necessary to meet the criteria for homogeneous plastic deformation. However, as the temperature rises above 225 °C, the formability of Mg increases due to a decrease in the critical resolved shear stress [23].

The texture formed during the rolling process offers valuable insights into the material's behavior and mechanical properties. This research aims to examine these characteristics using electron backscatter diffraction (EBSD) and X-ray diffraction (XRD). XRD has been widely used in various studies to analyze the lattice behavior of crystallographic materials and to determine the phase composition through diffraction intensity. In this study, XRD will help to identify whether a preferred orientation is achieved through conventional rolling and verify the presence of stress-induced secondary phases in the rolled samples as a result of plastic deformation. EBSD is an excellent tool for providing detailed crystallographic data and orientation. Within the parameters of this research, we will use EBSD to observe changes in the material's texture and orientation induced by the rolling process. This combination of XRD and EBSD techniques will allow for a comprehensive analysis of the material's behavior and texture following rolling.

As for the present investigation, the aim is to evaluate the effects of the rolling parameters on the structure and strain rate of lightweight materials, with the objective of developing a process map that prioritizes strain rate control over the traditionally used reduction percentage. By focusing on the strain rate control, this study seeks to preserve the ductility of lightweight materials, mitigate strain hardening effects, and promote texture development while enhancing the strength properties. The findings of this research could improve material performance in various applications, particularly in industries in which weight reduction and strength are crucial. Advancing the understanding of strain rate control addresses a specific need in materials science and engineering.

The novelty of this research lies in its approach to understanding the texture and mechanical properties of lightweight alloys, specifically Mg-Al and Ti-6Al-4V, using advanced analytical techniques like electron backscatter diffraction (EBSD) and X-ray diffraction (XRD). These techniques provide detailed insights into crystallographic texture and phase composition changes induced by the rolling process, which are critical for optimizing the material performance. By focusing on Mg-Al and Ti-6Al-4V, this research addresses materials that are important for the automotive, aerospace, and medical industries. Understanding how rolling processes affect these lightweight alloys could lead to enhanced performance in applications in which weight and strength are paramount.

Controlling the rolling temperature is crucial to avoid the formation of undesirable phases, such as the brittle γ-$Al_{12}Mg_{17}$ phase in Mg-Al alloys and the martensitic transformation in Ti-6Al-4V. Careful temperature management is essential for preserving material integrity while investigating deformation mechanisms. Enhancing the strength and ductility of lightweight alloys through plastic deformation processes can improve material sustainability and durability while maintaining a low weight. By addressing the gap in the current literature regarding the optimization of rolling processes for lightweight materials, this study contributes valuable insights to the field, offering a pathway to optimizing these alloys for high-performance applications in which weight reduction is critical.

2. Materials and Methods

This study utilized three different lightweight alloys with varying compositions. T5 commercial-grade titanium (Ti-6Al-4V) was cut from a commercially procured rolled sheet into strips measuring 25.4 × 152.4 mm with a thickness of 1.6 mm. The other two specimen types were Mg-Al alloys with aluminum contents of 6 and 9 wt%. Both Mg-6Al and Mg-9Al were cast as slabs in-house, with their chemical compositions listed in Table 1. To avoid the formation of the brittle

γ-$Al_{12}Mg_{17}$ phase, the Mg-Al alloys were fully solutionized. Four strips measuring 21.6 × 119.4 mm were cut from Mg-6Al, and four strips measuring
19.1 × 106.7 mm were cut from Mg-9Al, both with an approximate thickness of 3 mm. All the samples were roughly polished to remove surface roughness and sharp edges from the cutting process.

Table 1. Rolling parameters.

Materials	Speed Ratio	Preheating Temperature (°C)	Initial Thickness (mm)	Thickness Reduction per Pass	Total Thickness Reduction	Number of Passes
Mg-6Al	1:1	315	2.30	15%	56.5%	5
Mg-9Al	1:1	400	2.40	15%	58.3%	5
Ti-6Al-4V	1:1	650	1.60	5%	37.5%	9

After polishing, measurements of each specimen were recorded and listed in Table 1. Each specimen underwent warm working through conventional rolling, using work rolls with a diameter of 50 mm, a rolling speed of 1.0 m/min, and a 1:1 speed ratio between the rolls. The rolling parameters were preset for each specimen based on the initial thickness, reduction percentage per pass, and material properties. The target final thickness for each specimen was 1 mm. The initial thicknesses were 2.3 mm for Mg-6Al, 2.4 mm for Mg-9Al, and 1.6 mm for Ti-6Al-4V. The reduction percentages per pass were 15% for Mg-Al alloys and 5% for Ti-6Al-4V, set to prevent defects such as cracking or spallation [24,25]. These parameters determined the number of passes needed for each specimen: 5 passes for Mg-Al alloys and 9 for the Ti alloy.

Prior to each pass, the specimens were preheated for 5 min to maintain the rolling temperature. Mg-Al specimens were solution-treated by heating above the γ phase region to avoid undesirable phases, with preheating temperatures of 315 °C for Mg-6Al and 400 °C for Mg-9Al, to prevent the $Al_{12}Mg_{17}$ phase [2]. The Ti-6Al-4V specimens were preheated at 650 °C to prevent martensitic phase transformation [9]. The conventional roller used in this experiment had a rolling temperature limit of 300 °C. Consequently, the temperature during the rolling process was maintained at a constant 300 °C.

By controlling the rolling temperature, the formation of undesirable phases, such as the brittle γ-$Al_{12}Mg_{17}$ phase in Mg-Al alloys and martensitic transformation in Ti-6Al-4V, are avoided. This careful temperature management is essential for preserving the material integrity while investigating deformation mechanisms.

One of the four Mg-6Al samples was used as a dummy sample to calibrate, preheat, and prep the roller for experimentation, leaving the remaining three samples for data analysis. The sample thickness of each specimen type was measured after each pass and averaged. The final pass for each sample was a double pass in which the thickness was reduced to the final size, and then the specimen was flipped and passed through again without additional thickness reduction. After rolling, each specimen was quenched in room-temperature water for 5 s to preserve the material's microstructure. It is important to note that there was no significant change in the chemical composition of each sample after rolling. Table 2 shows the chemical composition of each alloy before and after rolling.

Table 2. Material composition.

Materials	Element	Pre-Rolled Weight %	Post-Rolled Weight %
Mg-6Al	Mg	92.69	92.51
	Al	7.31	7.49
Mg-9Al	Mg	89.25	89.25
	Al	10.75	10.75
Ti-6Al-4V	Ti	85.34	86.92
	Al	6.39	6.55
	V	6.19	6.53

The post-rolled samples were prepared for microscopic and spectroscopic analysis. This involved a series of grinding and polishing steps, conducted using a MultiPrep System polisher

(Allied High Tech Products, Inc, Compton, CA, USA). For etching, the Mg-Al samples were treated with a 2.5% nitric acid solution for 30 s, while the Ti samples were etched using a 10% HF solution for 10 s. The rolling normal direction of each sample was then examined using a Zeiss Imager M2 optical microscope.

To observe the phase composition, a Hitachi SU8000 scanning electron microscope (SEM, Tokyo, Japan) equipped with an Oxford Instruments Aztec electron backscattering diffraction (EBSD, Abingdon, UK) CMOS EBSD detector was used. EBSD data analysis was carried out with Oxford Instruments Aztec software (version 6.0).

For the analysis of the crystal direction and orientation, a Bruker D8 Discover X-ray diffraction (XRD, Billerica, MA, USA) machine was employed. The XRD measurements were taken over a range of 30° to 80° with a scanning speed of 2 s per step and a step size of 0.0172°. The resulting XRD data were processed using Bruker Diffrac Eva software (version 5.2) to accurately determine the crystal structures present in the samples.

3. Results

The final average thicknesses achieved for the rolled Mg-6Al, Mg-9Al, and Ti-6Al-4V samples were 0.98 mm, 0.95 mm, and 0.95 mm, respectively, corresponding to total thickness reductions of 57.6%, 60.4%, and 40.6%. Throughout the rolling process, each specimen remained intact and exhibited no visible defects. However, the strain rate increased with each pass. Figure 1 presents the true strain rate for each pass, where the numbers on each point indicate the draft per pass (in mm), defined as the difference between the initial and final thickness.

According to the figure, there is a noticeable peak in the strain rate during the final pass for Mg-9Al and Ti-6Al-4V. This peak is likely attributed to the double pass applied during the final rolling reduction. Reorienting the sample and passing it twice without reducing the thickness provides an opportunity for dislocations to move in a different direction compared to the previous rolling path, thus contributing to the observed strain rate increase. This study highlights the importance of controlling the strain rate during the rolling process to maintain the material's ductility and manage strain hardening. By understanding the relationship between draft per pass and strain rate, the process parameters can be optimized to enhance the mechanical properties of the rolled alloys. This detailed analysis of the strain

rate's behavior and its implications on the material properties highlights the significance of precise control in the rolling of lightweight materials.

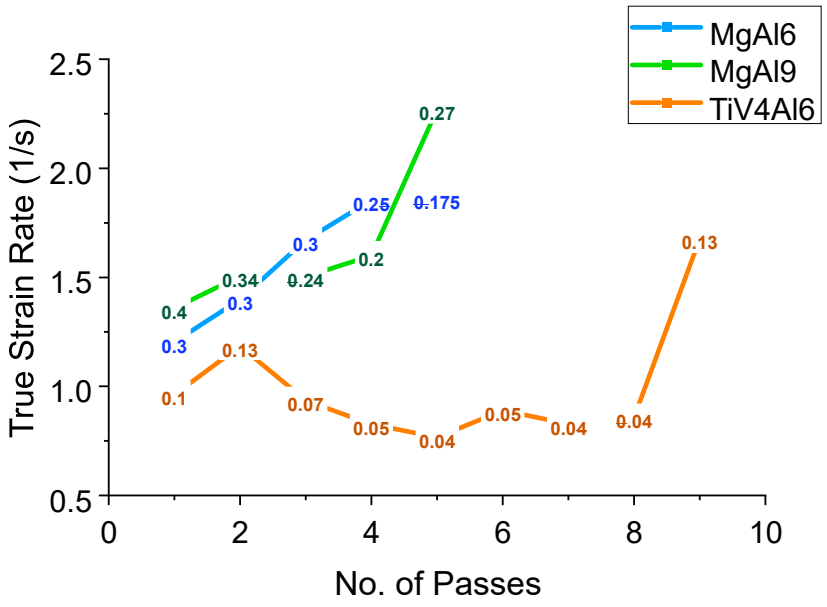

Figure 1. The true strain rate of each specimen per pass with draft values.

In Figure 1, it is observed that the Mg-Al samples experienced an increase in the strain rate per pass with fluctuating draft values. For the Ti-6Al-4V sample, the strain rate was more constant with each pass. This can be credited to two factors: firstly, the 5% thickness reduction per pass for Ti-6Al-4V, contrasting with the 15% reduction applied to the Mg-Al samples; secondly, the greater hardness of Ti-6Al-4V. From this result, it can be concluded that reducing the draft decreases the strain rate in the Ti-6Al-4V samples. Reducing the draft in Mg-Al presents more of a challenge considering it is a much softer metal allowing for more atomic dislocations. This finding underscores the complex interplay between the material properties and the process parameters in determining the strain rate during rolling.

3.1. Microstructure Evolution

Figure 2 shows the microstructure of all the samples before and after rolling. For the Mg-Al alloys, the average grain sizes of the solution-treated specimens were larger at about 53.1 µm for Mg-6Al and 64.4 µm for Mg-9Al. The increased amount of Al content increases the grain size in the Mg-Al alloys. After rolling, the average grain size of Mg-6Al was about 2.5 µm and that for Mg-9Al was about 4.4 µm. For the Mg-Al alloys, the reduction in grain size was greater than 90%. This was not the case for the Ti-6Al-4V specimen. After rolling the Ti alloys, the average grain size reduced by less than 5% with a value, prior to rolling, of about 2.7 µm and 2.6 µm after rolling. This reduction in grain size is considered to be negligible.

Through the EBSD analysis, shown in Figure 3, it was observed that the preferred orientation of crystals was achieved in all rolled specimens. Prior to rolling, the solutiontreated Mg-Al alloys crystals were large and randomly oriented. Appendix A contains the sample orientation that correspond to the crystal orientation of the phases present in each specimen. The rolled Mg-Al alloys have a preferred orientation of the (0001) plane, which corresponds with basal slip. There was also evidence of stressors within the larger grains of the rolled Mg-Al samples. The phase most present in the Mg-Al alloys was the magnesium phase, and a phase change did not occur as a result of the rolling process. For the Ti alloy,

$$\bar{1}\,\bar{2}$$

the preferred orientation of (1210) was achieved but with less concentration than that of the Mg-Al alloys. Before rolling, Ti-6Al-4V consisted primarily of the Ti hexagonal phase with strong phases of vanadium intermingled between the phases of Ti. After rolling, the vanadium phase was more disbursed through the dominating Ti hexagonal phase in smaller concentrations.

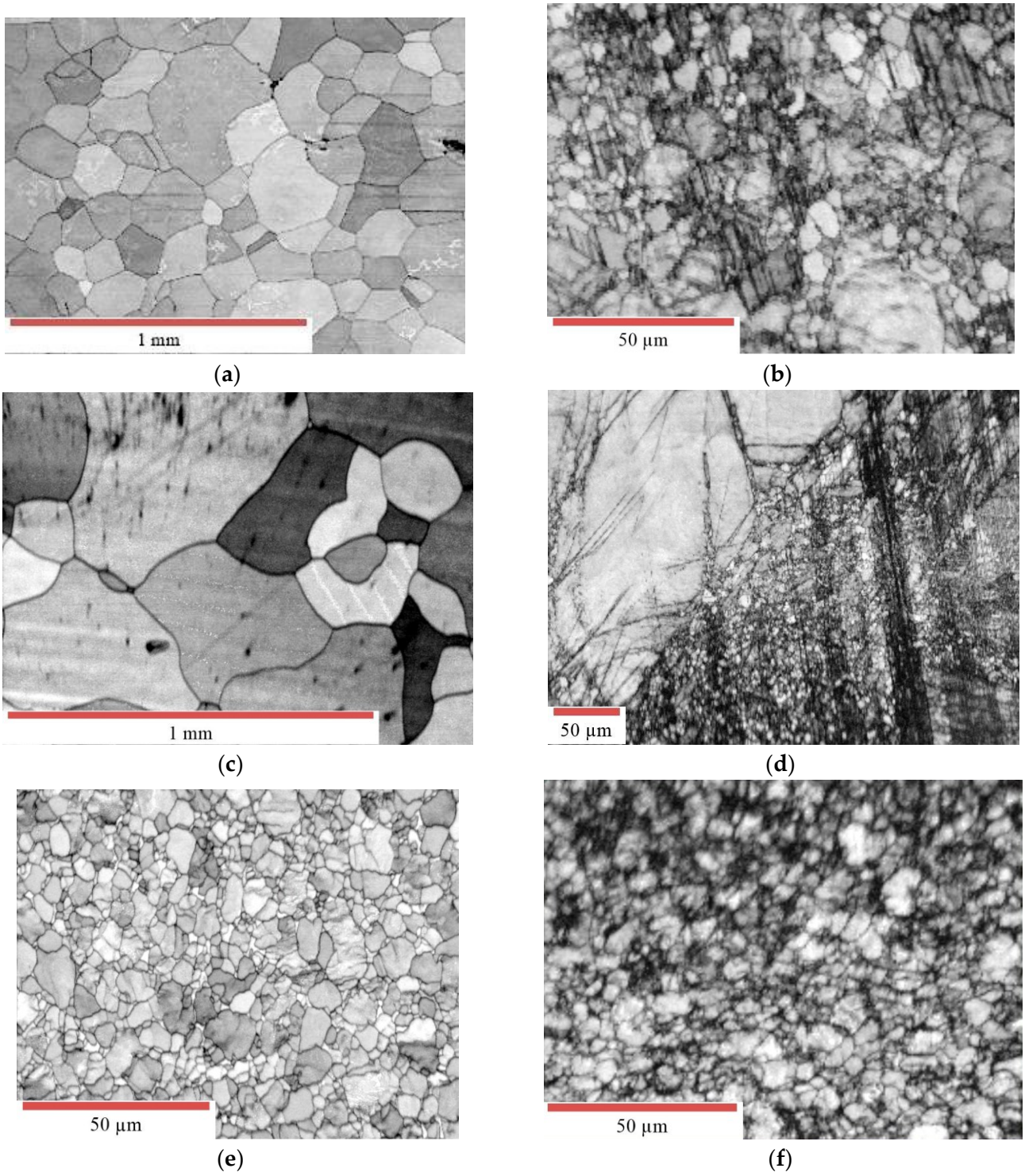

Figure 2. Grain size of material before and after rolling: (**a**) Mg-6Al, solution treated; (**b**) Mg-6Al, rolled; (**c**) Mg-9Al, solution treated; (**d**) Mg-9Al, rolled; (**e**) Ti-6Al-4V; (**f**) Ti-6Al-4V, rolled.

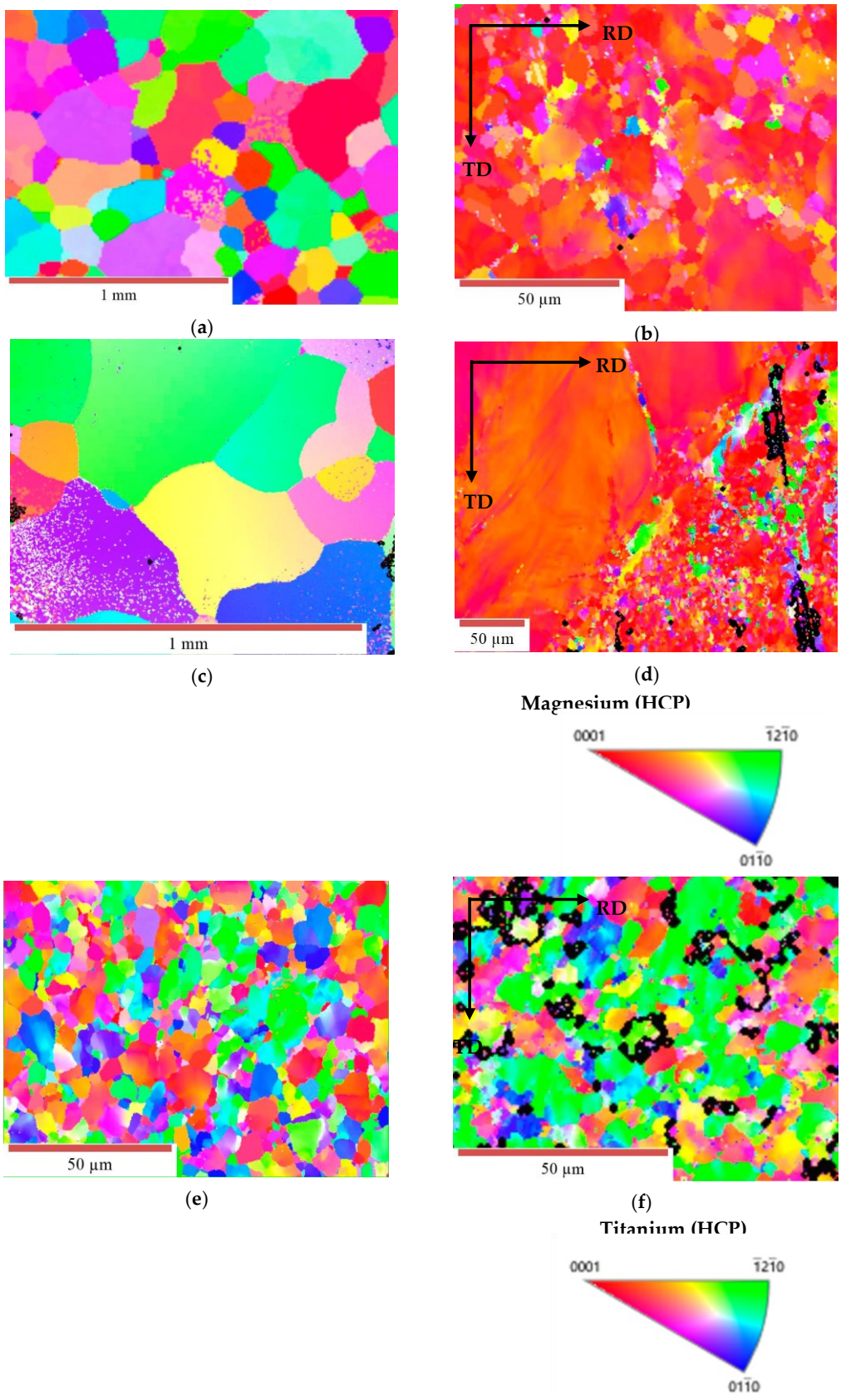

Figure 3. EBSD crystallographic orientation of the normal surface of samples before and after rolling: (**a**) Mg-6Al, solution treated; (**b**) Mg-6Al, rolled with a (0001) preferred planar orientation; (**c**) Mg-9Al, solution treated; (**d**) Mg-9Al, rolled with a (0001) preferred planar orientation; (**e**) Ti-6Al-4V;

(**f**) Ti-6Al-4V, rolled with a primary preferred planar orientation of (1210).

3.2. XRD Analysis

Figure 4 depicts the XRD diffraction patterns of the Mg-6Al, Mg-9Al, and Ti-6Al-4V alloys before and after rolling. The peaks of each of the samples were matched to the crystallographic database for Mg and Ti patterns, respectively. Each peak corresponds to a planar direction of a certain intensity. In all the samples, the number of diffraction peaks did not significantly change. The peaks observed on the solution-treated Mg-Al alloys were generally narrow indicating large crystallite structures. After rolling Mg-6Al, the rolled sample peak intensity significantly dropped at about 32° 2θ, while the peak intensity around 35° 2θ shot up. This increased intensity at 35° 2θ suggests that there is a preferred orientation of (0002) as a result of rolling Mg-6Al. A similar phenomenon occurred in the Mg-9Al sample in that there was an intensity increase at 35° 2θ, once again suggesting a preferred orientation along the (0002) plane. After rolling, the peak intensity at 57° 2θ for solution-treated Mg-9Al decreased to a negligible level. For the Ti-6Al-4V alloys, the XRD data displayed broader peaks, indicating very small crystallite structures. The intensity of each peak broadened and significantly increased. The broadening of each peak can be attributed to the occurrence of non-uniform strain as a result of rolling. For the rolled Ti-6Al-4V sample, the peak intensity increased at about 38° and 40°, suggesting that the crystals were becoming smaller and follow a more preferred direction of (0002) and (0111). The ratios between the 38° and 40° peaks before rolling were about 3:2 and 2:1 after rolling.

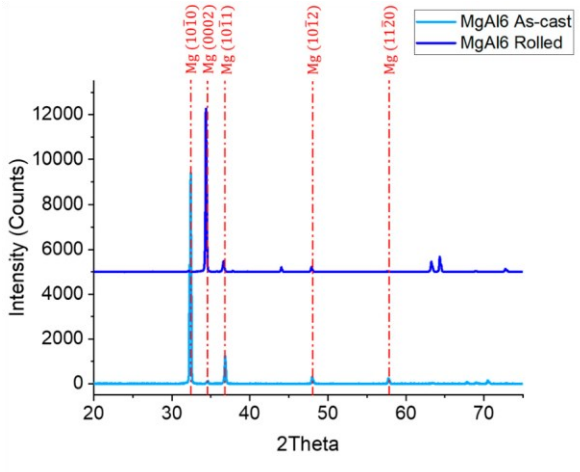

(**a**)

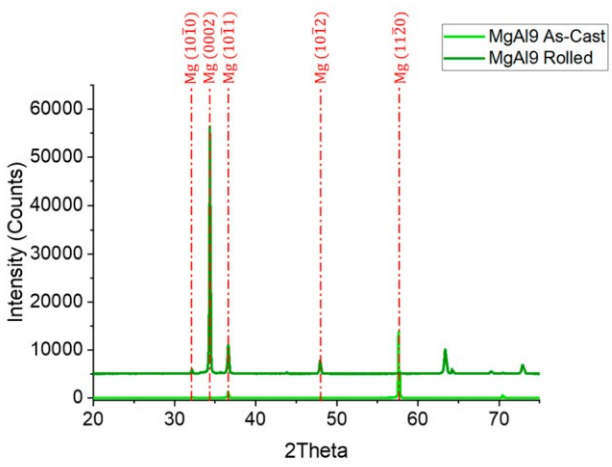

(**b**)

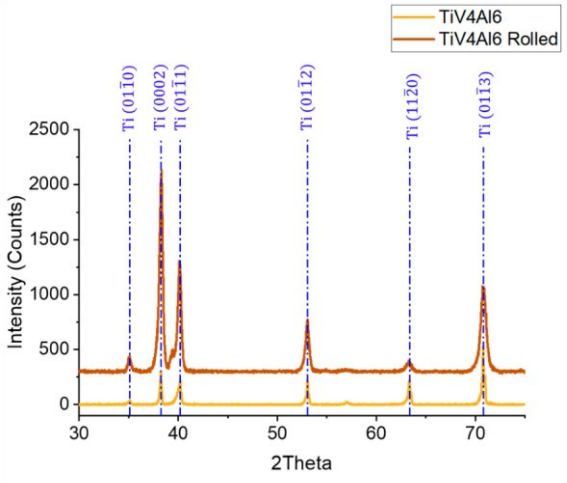

(**c**)

Figure 4. XRD data of samples before and after rolling: (**a**) Mg-6Al, solution treated vs. rolled; (**b**) Mg-9Al, solution treated vs. rolled; (**c**) Ti-6Al-4V as procured vs. rolled.

3.3. Formatting of Mathematical Components

Figure 5 depicts the free-body diagram of the forces applied to the rolled material by the roll. The volume of the rolled material remains the same as there is no material being added or taken away.

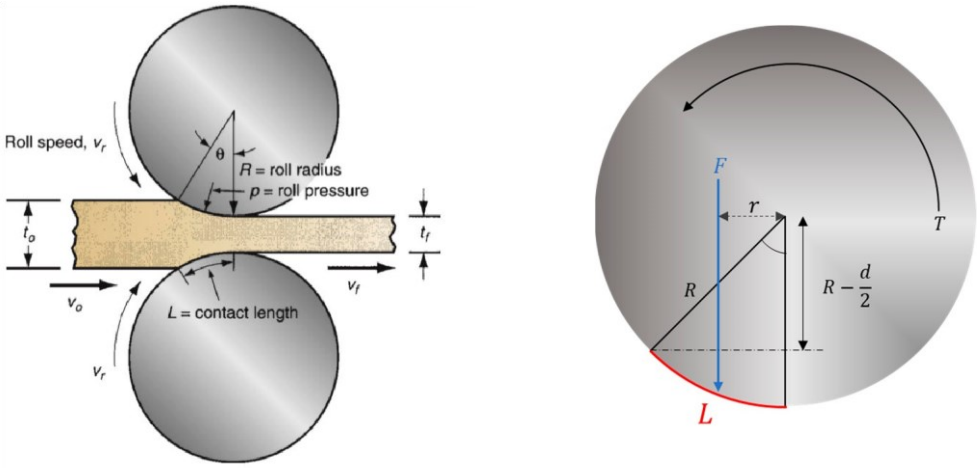

(**a**) (**b**)

Figure 5. The free-body diagram of conventional rolling: (**a**) image from Fundamentals of Modern Manufacturing: Materials, Processes, and Systems textbook [10]—forces exerted on the sample by both top and bottom rollers; (**b**) forces exerted by a single roller.

Variables that impact the true strain rate include the reduction percentage, temperature, and roll speed. The draft d of a rolled material is the difference in the thickness before and after rolling. Reduction r is often represented as a percentage and is the draft divided by the initial thickness.

$$r = \frac{d}{t_0} = \frac{t_0 - t_f}{t_0} \quad (1)$$

The experiment was recalculated so that the strain rate stayed constant. The equation for the true strain rate is as follows:

$$\dot{\epsilon} = \frac{v}{L} \ln \frac{t_0}{t_f} \quad (2)$$

where v is velocity, L is contact length, and t_f and t_0 are final and initial thicknesses. The contact length can be expressed in terms of thickness as follows:

$$L = \sqrt{Rd} = \sqrt{R\left(t_o - t_f\right)} \quad (3)$$

where R is the radius of the rolls and d is the draft. In order to manipulate the strain rate, the effects of changes in the draft size or reduction percentage and velocity were analytically observed.

4. Discussion

The expectation was to keep a constant percentage of reduction for each pass; however, the reduction percentage varied and spiked on the last pass of each specimen. This anomaly can be explained by the heightened dislocation density resulting from the final pass being a double pass, leading to increased strain hardening due to a flipped specimen orientation. It was also observed that increases in the percentage of reduction with each pass were correlated with higher strain rates. With each pass, the ability to stay true to the constant reduction percentage became more

of a challenge because, with each pass, the strain increases, which limits dislocation. It was also concluded through calculation that, even if a constant percentage were maintained, the strain rate would still increase with each pass. Increasing the strain rate for each material increases the likelihood of failure. From this, it can be hypothesized that, if the rolling process is controlled keeping a constant strain rate, it can ensure that no damage occurs during the process.

A process map was developed in order to control the strain rate for each pass. The variables that affect the true strain rate are the temperature, roll speed, and the initial and final thickness of the material. The temperature must remain constant in order to avoid phase transformation. Therefore, for the purposes of developing the process map, the factors that may vary are the roll velocity and the material thickness or draft. If the roll speed is too fast, there is more possibility of a fracture due to the spring back effect as well as the formation of twin structure especially for the much softer Mg-Al alloys. Because of this, the velocity domain was observed within the ranges of 1–2.5 m/min. The developed process map is depicted in Figure 6a. It can be observed that, by maintaining a constant strain rate, we can avoid failure and have more control over the rolling process. Figure 6 also shows a breakdown of the process map in terms of the daft and the reduction percentage, respectively.

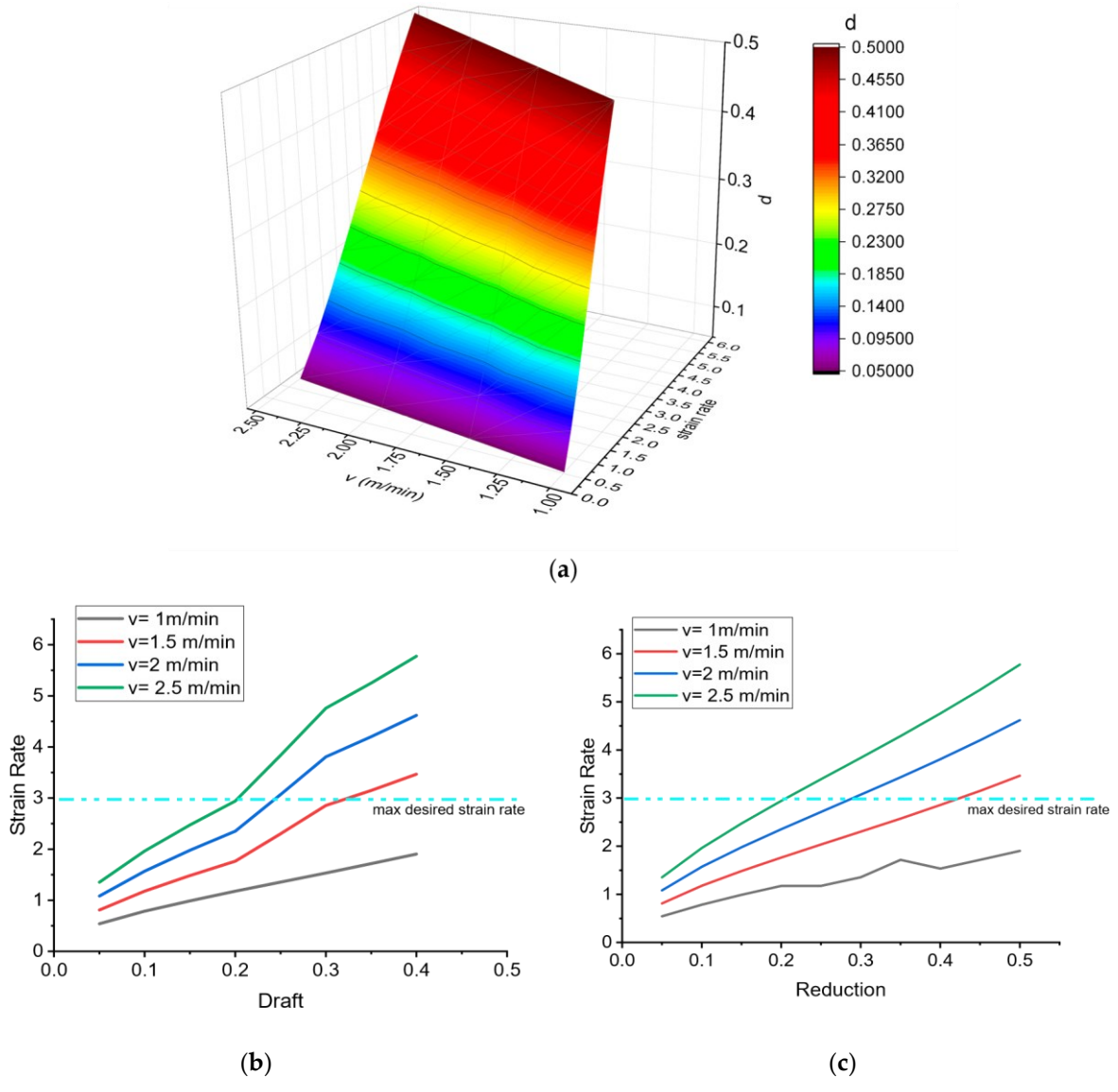

Figure 6. Controlling rolling process by strain rate. (**a**) Process map of velocity and draft effect on strain rate, (**b**) draft vs. strain rate for various velocities, (**c**) reduction percentage vs. strain rate for various velocities.

The proposed model will help control the strain rate by selecting the appropriate velocity and draft for each pass. By selecting a velocity and draft that corresponds to the desired strain rate, the strain rate can be held constant retaining more ductility and reducing the likelihood of failure during processing. This ensures that we can strengthen material through a cold working process without compromising the material's integrity.

5. Conclusions

The conventional rolling process significantly reduced the grain size in the Mg-Al system by over 90% at ~58% cold work (CW) and in the Ti-6Al-4V alloy by 4% at ~41% CW. This reduction in grain size, coupled with an increase in the dislocation density and strain after each pass, indicates that strain hardening is occurring and generating texture. Texture (preferred plane orientation) was observed in all alloys after rolling.

This study aimed to evaluate the impact of the texture on the strain rate and to identify process parameters to maintain a more consistent strain rate. This goal was achieved through the development of a process map that assesses the parameters contributing to strain values. This study specifically investigates how conventional rolling affects the texture of Mg-Al and Ti-6Al-4V alloys. By analyzing the texture formation and its implications on mechanical properties, this research provides insights that are critical for optimizing rolling processes in industrial applications. It not only investigates the microstructural changes of the Mg-Al and Ti-6Al-4V alloys but it also develops a process map that correlates rolling parameters (such as temperature, strain rate, and reduction percentage) with the resulting strain and texture. This practical tool can guide future processing techniques to achieve the desired material properties.

The proposed process map can be utilized in future studies and, given that the draft is directly associated with the reduction percentage, this process can potentially be modified and applied to other severe plastic deformation processes. This study can also be extended to include mechanical studies such as hardness and strength evaluations. Future research may investigate the effects of maintaining a constant strain rate during the rolling process on mechanical properties like strength and hardness.

Author Contributions: Methodology, J.R. and Z.X.; Formal analysis, J.R.; Investigation, J.R.; Resources, S.F., Z.X. and J.S.; Data curation, J.R. and K.H.; Writing—original draft, J.R.; Writing—review & editing, J.R., S.F., Z.X., C.H. and K.H.; Supervision, S.F., Z.X. and C.H.; Project administration, J.S. All authors have read and agreed to the published version of the manuscript.

Funding: This research was funded by the National Science Foundation under Grant No. (NSF EEC2133630).

Data Availability Statement: The original contributions presented in the study are included in the article, further inquiries can be directed to the corresponding author.

Acknowledgments: This material is based on research sponsored by the Air Force Research Laboratory under agreement number FA8650-20-2-5853. The U.S. Government is authorized to reproduce and distribute reprints for government purposes notwithstanding any copyright notation thereon. The views and conclusions contained herein are those of the authors and should not be interpreted as necessarily representing the official policies or endorsements, either expressed or implied, of the Air Force Research Laboratory of the U.S. Government.

Conflicts of Interest: The authors declare no conflict of interest.

Appendix A

The samples were positioned on the sample mount with their normal direction perpendicular to the surface and the rolling the direction is along the *x*-axis as seen in Figure A1.

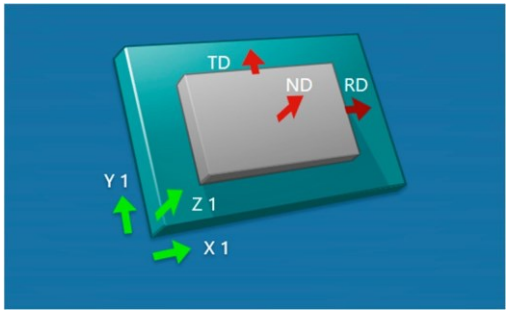

Figure A1. Sample orientation for EBSD analysis.

References

1. Gupta, M.; Sharon, N.M. *Magnesium, Magnesium Alloys, and Magnesium Composites*; John Wiley & Sons, Inc.: Hoboken, NJ, USA, 2010.
2. Mezbahul-Islam, M.; Mostafa, A.O.; Medraj, M. Essential Magnesium Alloys Binary Phase Diagrams and Their Thermochemical Data. *J. Mater.* **2014**, *2014*, 704283. [CrossRef]
3. Murugesan, R.; Venkataramana, S.H. Influence of Alloying Materials Al, Cu, and Ca on Microstructures, Mechanical Properties, And Corrosion Resistance of Mg Alloys for Industrial Applications: A Review. *ACS Omega* **2023**, *8*, 37641–37653. [CrossRef] [PubMed]
4. Zhang, L.; Cao, Y.B. Effect of Al content on the microstructures and mechanical properties of Mg–Al alloys. *Mater. Sci. Eng. A* **2008**, *508*, 129–133. [CrossRef]
5. Friedrich, H.E.; Mordike, B.L. Physical Metallurgy. In *Magnesium Technology: Metallurgy, Design Data, Apllications*, 1st ed.; Springer: Berlin/Heidelberg, Germany, 2006; pp. 63–107.
6. Sanamar, S.; Brokmeier, H.G. Formation of the intermetallic phases $Al_{12}Mg_{17}$ and Al_3Mg_2 during heating of elemental Al-Mg composites studied by high-energy X-ray diffraction. *J. Alloys Compd.* **2022**, *911*, 165114. [CrossRef]
7. Ducato, A.; Fratini, L.; La Cascia, M.; Mazzola, G. An Automated Visual Inspection System for the Classification of the Phases of Ti-6Al-4V Titanium Alloy. In Proceedings of the 15th International Conference on Computer Analysis of Images and Patterns, York, UK, 27–29 August 2013; pp. 362–369.
8. Blanco, D.; Rubio, E.M.; Marin, M.M.; Davim, J.P. Advanced materials and multi-materials applied in aeronautical and automotive fields: A systematic review approach. *Procedia CIRP* **2021**, *99*, 196–201. [CrossRef]
9. Macleod, S.G.; Errandonea, D.; Cox, G.A.; Cynn, H.; Daisenberger, D.; Finnegan, S.E.; McMahon, M.I.; Munro, K.A.; Popescu, C.; Storm, C.V. The phase diagram of Ti-6Al-4V at high-pressures and high-temperatures. *J. Phys. Condens. Matter* **2021**, *33*, 154001. [CrossRef] [PubMed]
10. Deng, B.; Dai, Y.; Lin, J.; Zhang, D. Effect of Rolling Treatment on Microstructure, Mechanical Properties, and Corrosion Properties of WE43 Alloy. *Material* **2022**, *15*, 3985. [CrossRef] [PubMed]
11. Zhu, S.Q.; Yan, H.G.; Chen, J.H.; Wu, Y.Z.; Liu, J.Z.; Tian, J. Effect of twinning and dynamic recrystallization on the high strain rate rolling process. *Scr. Mater.* **2010**, *63*, 985–988. [CrossRef]
12. John, M.; Ralls, A.M.; Dooley, S.C.; Thazhathidathil, A.K.V.; Perka, A.K.; Kuruveri, U.B.; Menezes, P.L. Ultrasonic Surface Rolling Process: Properties, Characterization, and Applications. *Appl. Sci.* **2021**, *11*, 10986. [CrossRef]
13. Liu, C.; Liu, D.; Zhang, X.; He, G.; Xu, X.; Ao, N.; Ma, A.; Liu, D. On the influence of ultrasonic surface rolling process on surface integrity and fatigue performance of Ti-6Al-4V alloy. *Surf. Coat. Technol.* **2019**, *310*, 24–34. [CrossRef]
14. Raabe, D. Deformation Processing. In *Encyclopedia of Condensed Matter Physics*; Elsevier: Amsterdam, The Netherlands, 2005; pp. 387–395.
15. Groover, M.P. *Fundamentals of Modern Manufacturing: Materials, Processes, and Systems*, 5th ed.; John Wiley & Sons, Inc.: Hoboken, NJ, USA, 2013; pp. 419–421.
16. Humphreys, F.J.; Hatherly, M. *Recyrstallization and Related Annealing Phenomena*, 2nd ed.; Elsevier: Amsterdam, The Netherlands, 2004.
17. Chapuis, A.; Liu, Q. Simulations of texture evolution for HCP metals: Influence of the main slip systems. *Comput. Mater. Sci.* **2015**, *97*, 121–126. [CrossRef]
18. Wang, H.W.; Xue, E.S.; Nan, X.L.; Yue, T.; Wang, Y.P.; Jiang, Q.C. Influence of grain size on strain rate sensitivity in rolled Mg–3Al–3Sn alloy at room temperature. *Scr. Mater.* **2013**, *68*, 229–232. [CrossRef]
19. Capolungo, I.; Beyerlein, I.J.; Wang, Z.Q. The role of elastic anisotropy on plasticity in hcp metals: A three-dimensional dislocation dynamics study. *Model. Simul. Mater. Sci. Eng.* **2010**, *18*, 16. [CrossRef]
20. Ma, Z.A.; Tang, X.Z.; Mao, Y.; Guo, Y.F. The Plastic Deformation Mechanisms of hcp Single Crystals with Different Orientations: Molecular Dynamics Simulations. *Material* **2021**, *14*, 773. [CrossRef] [PubMed]
21. Tehranchi, A.; Yin, B.; Curtin, W.A. Solute strengthening of basal slip in Mg alloys. *Acta Mater.* **2018**, *151*, 56–66. [CrossRef]
22. Yapici, G.G.; Karaman, I. Common trends in texture evolution of ultra-fine-grained hcp materials during equal channel angular extrusion. *Mater. Sci. Eng. A* **2009**, *503*, 78–81. [CrossRef]

23. Mackenzie, L.W.F.; Pekguleryuz, M. The influences of alloying additions and processing parameters on the rolling microstructures and textures of magnesium alloys. *Mater. Sci. Eng. A* **2008**, *480*, 189–197. [CrossRef]
24. Zhang, H. Study on Dynamic Recrystallization and Improving Mechanical Properties of Mg-*x*Al(*x* = 6,9) Alloy through Differential Speed Rolling. Ph.D. Thesis, North Carolina A&T State University, Greensboro, NC, USA, 2022.
25. Yu, F.; Zhang, Y.; Kong, C.; Yu, H. Microstructure and mechanical properties of Ti-6Al-4V alloy sheets via room-temperature rolling and cryorolling. *Mater. Sci. Eng. A* **2022**, *834*, 142600. [CrossRef]